atmosphere

MDPI

Review

N_2O Emissions from Aquatic Ecosystems: A Review

Huixiao Pan [1], Zheyan Zhou [1], Shiyu Zhang [1], Fan Wang [1,2,3] and Jing Wei [1,2,3,*]

[1] School of Atmospheric Sciences, Sun Yat-sen University, Zhuhai 519082, China; panhx8@mail2.sysu.edu.cn (H.P.)
[2] Guangdong Province Key Laboratory for Climate Change and Natural Disaster Studies, Sun Yat-sen University, Zhuhai 519082, China
[3] Southern Marine Science and Engineering Guangdong Laboratory (Zhuhai), Zhuhai 519082, China
* Correspondence: weij53@mail.sysu.edu.cn

Abstract: Emissions of nitrous oxide (N_2O) from aquatic ecosystems are on the rise due to the dramatic increase in global reactive nitrogen input by anthropogenic activities (e.g., agricultural nitrogen fertilizer use). However, uncertainties exist in the estimation of aquatic N_2O budgets due to limited knowledge of mechanisms involved in aquatic N_2O emissions, as well as the N_2O flux measurements and modelling. To give a full picture of aquatic N_2O emissions, this review discusses the biotic and abiotic mechanisms involved in aquatic N_2O emissions, common methods used in aquatic N_2O flux measurements (including field measurement methods and formula simulation methods), and alternatives for aquatic N_2O budget estimation. In addition, this review also suggests that stable isotope technology is promising in the application of aquatic N_2O source partitioning.

Keywords: nitrous oxide; aquatic ecosystem; isotope techniques; mechanisms

1. Introduction

Nitrous oxide (N_2O), whose single-molecular global warming potential is 273 times (100-year timescale) greater than carbon dioxide, is the third most important long-term greenhouse gas (LLGHG) and accounts for about 7% of the total radiative forcing of LLGHG in 2020 [1,2]. N_2O has a long residence time of 110–180 years in the atmosphere [3]. N_2O is stable in the troposphere, but when it escapes into the stratosphere, it is photolyzed into NO radical by ultraviolet light, which further destroys the stratospheric ozone layer [4,5]. After the prohibition of the usage of chlorofluorocarbon in The Montreal Protocol on Substances that Deplete the Ozone Layer, N_2O has become the most important ozone-depleting substance currently being emitted [4,5].

N_2O emissions increased rapidly during the Industrial Revolution [6], mainly due to the increased reactive nitrogen (Nr) input through the Haber–Bosch process [7,8]. According to the latest field network observation data, the global mean atmospheric N_2O concentration reached a new high (333.2 $\pm$ 0.1 ppb) in 2020, which is 123% of the pre-industrial level, and is still increasing at an average annual growth rate of 0.25% [2].

Aquatic ecosystems, including inland waters, estuaries, and oceans, have long been considered as net N_2O sources [9,10]. To meet the food demand of the dramatically growing world population, the application of chemical fertilizers increased from 11.46 Mt in 1961 to 113.29 Mt in 2020 to promote crop production (Figure 1). Only 15–70% of fertilizer N is taken up by plants, and some is leached into inland waters and further transported into estuaries and oceans [11–13]. Correspondingly, riverine N_2O emissions went through a growth of 91.5% from 0.15 Tg N_2O-N yr^{-1} in 1961 to 0.29 Tg N_2O-N yr^{-1} in 2016 [14]. It is estimated that the total N_2O emissions from global rivers and streams account for 10–15% of the total anthropogenic N_2O emissions [15]. More than 80% of anthropogenic nitrogen emissions from aquatic ecosystems come from the northern mid-latitudes, consistent with the geographic distribution of nitrogen use and population [16]. The annual N_2O

check for updates

Citation: Pan, H.; Zhou, Z.; Zhang, S.; Wang, F.; Wei, J. N_2O Emissions from Aquatic Ecosystems: A Review. *Atmosphere* **2023**, *14*, 1291. https://doi.org/10.3390/atmos14081291

Academic Editor: Hans Osthoff

Received: 14 July 2023
Revised: 10 August 2023
Accepted: 12 August 2023
Published: 15 August 2023

emissions of the source streams and lakes are 0.36 and 0.52 Tg N_2O yr^{-1}, respectively, which are affected by the discharge of wastewater from agricultural activities, human life, and industrial production [10].

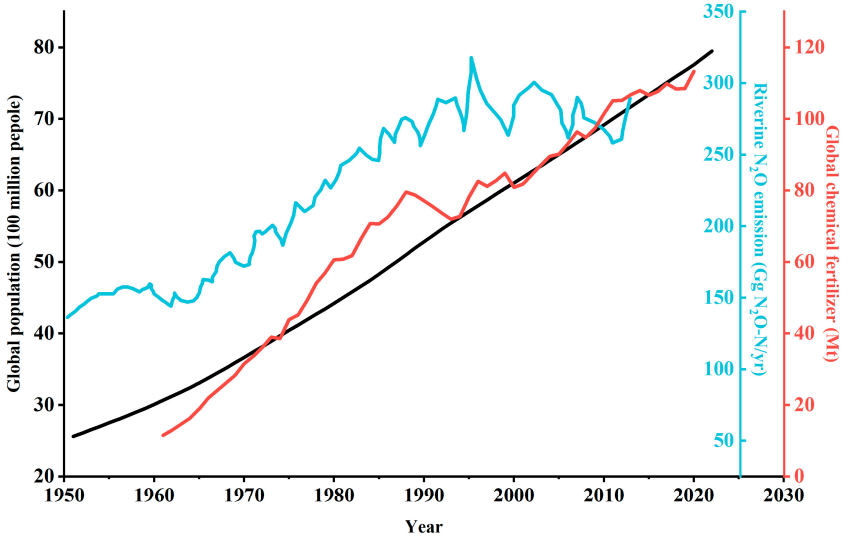

Figure 1. Trends of global population, fertilizer application, and global riverine N_2O emission. Riverine N_2O emission data from Yao et al., 2020 [14]; global population historical data from world-population; global fertilizer application data from FAOSTAT.

The global biogeochemical cycles of nitrogen in marginal oceans are being strongly interfered with, particularly in estuaries and coastal areas that serve as major transport channels between terrestrial and ocean ecosystems [17–19]. Although coastal areas account for only about 18% of the world's ocean area, they contribute to about 41% of global marine N_2O emissions [20–22]. The N_2O emission of the global coastal continental shelf areas affected by human activities was 0.6 Tg N_2O-N yr^{-1} [23]. The N_2O emissions from estuaries and coastal areas are 0.23 and 0.28 Tg N yr^{-1}, respectively, from 2007 to 2016 (Figure 2) [1,20], suggesting that coastal areas are an important source of global N_2O emissions.

The ocean is the second natural source of N_2O, but with the increase in atmospheric deposition of nitrogen compounds, the anthropogenic N input to the ocean is 1 Tg N yr^{-1} [24] and the Intergovernmental Panel on Climate Change (IPCC) assumed that the marine N_2O emissions range from 2.5 to 4.3 Tg N yr^{-1} with an average of 3.4 Tg N yr^{-1} from 2007 to 2016 (Figure 2) [1,25–27]. The global ocean contribution to N_2O emissions is estimated to be between 10% and 53%, with an average of 21%, but ongoing environmental changes are affecting ocean N_2O cycling and emissions to the atmosphere [28,29]. Although it is clear that the ocean is a major natural contributor of N_2O to the atmosphere, quantitative estimates remain uncertain [28,30,31].

This review aims to summarize the current state of knowledge of the role of aquatic ecosystems (inland waters–coastal regions–oceans) in global N_2O emissions and discuss methods of flux measurement and budget quantification, interpret mechanisms involved in N_2O production, and point out the power of stable isotope techniques in N_2O source partitioning.

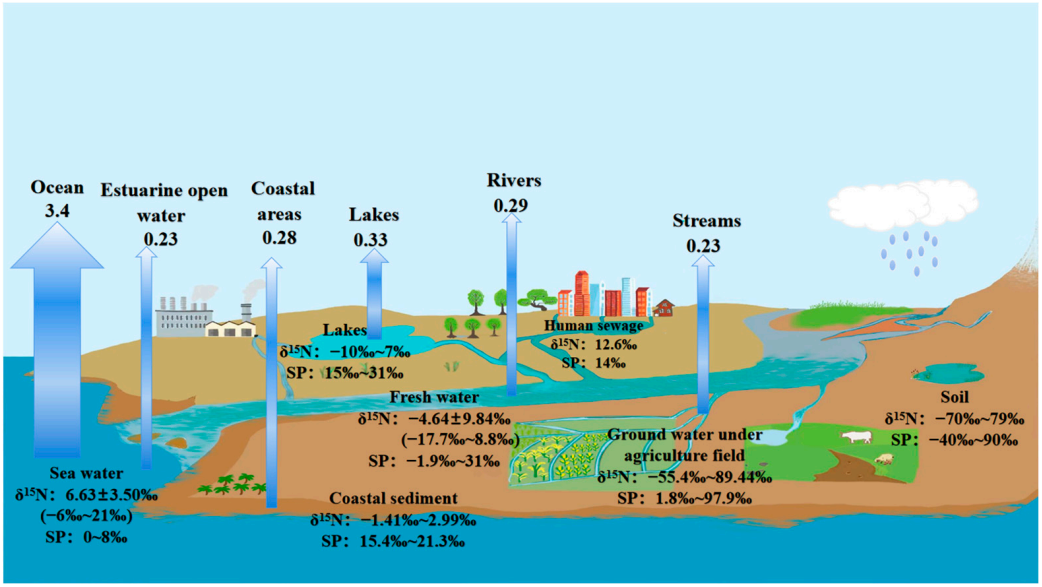

Figure 2. The N_2O budgets of different aquatic ecosystems and their isotopic values. The N_2O emission data of each aquatic ecosystem in units of Tg N_2O-N yr^{-1} [1,10,20]. The $\delta^{15}N$ isotope value in the figure represents the isotope ratio of ^{15}N and ^{14}N, and the site preference (SP) represents the enrichment difference between the proximal N and distal N of the O atom in the N_2O molecule; data derived from [32–36].

2. Mechanisms Involved in N_2O Production

2.1. Biological Pathways

N_2O production refers to the conversion of any other N species into N_2O [37]. In aquatic ecosystems, there are five different microbe-mediated pathways that are important for N_2O production (Figure 3): (1) Nitrification is catalyzed by ammonia-oxidizing archaea (AOA) or ammonia-oxidizing bacteria (AOB). NH_4^+ is stepwise oxidized into hydroxylamine (NH_2OH) and nitrite (NO_2^-), which is further oxidized into NO_3^- by nitrite-oxidizing bacteria (NOB), and N_2O is produced as a by-product of NH_2OH oxidation [38]. (2) Denitrification includes bacterial denitrification and fungal denitrification. The former is usually an anaerobic dissimilatory reduction process of NO_3^- to NO_2^-, NO, N_2O, and N_2 with reductase enzymes of nitrate reductase (Nar), nitrite reductase (Nir), nitric oxide reductase (Nor), and nitrous oxide reductase (Nos), while the latter lacks the gene encoding N_2O reductase (NosZ) and fail to reduce N_2O to N_2. So far, the reduction of N_2O to N_2 by Nos during denitrification is the only known biological pathway of N_2O consumption [4]. (3) Nitrate reduced to ammonium (DNRA) is a process that is primarily driven by nitrate-reducing bacteria and nitrite-reducing bacteria; N_2O is produced as a byproduct of NO_2^- reduction [39]. (4) Nitrifier denitrification refers to the process in which denitrification is conducted by nitrifiers instead of denitrifiers [40]. (5) Coupled nitrification and denitrification is the oxidation of NH_4^+ to NO_3^- under an aerobic or micro-oxygen environment and the reduction of NO_3^- to N_2O under anaerobic or hypoxic conditions [41–46].

Microbial nitrification and denitrification are biological pathways that contribute largely to aquatic N_2O production [47–49]. In heavily polluted estuaries, the contribution of nitrification and denitrification to N_2O emission ranges from 4.52% to 38.1% and from 61.9% to 80.3%, respectively [32,50]. The anoxic zone of the estuary accounts for 90% of the total estuarine N_2O production, which is very likely from denitrification [35,51,52]. The contribution of denitrification to total N_2O emissions is about 44%, 14%, 1%, and 11% in global continental shelves, marine oxygen minimum zones (OMZs), estuarine, and freshwater ecosystems (except groundwater), respectively [16]. When the estuary is affected by ocean acidification, N_2O release from the sediment is stimulated mainly by

bacterial denitrification, while in a neutral environment, N_2O production is dominated by fungi [53].

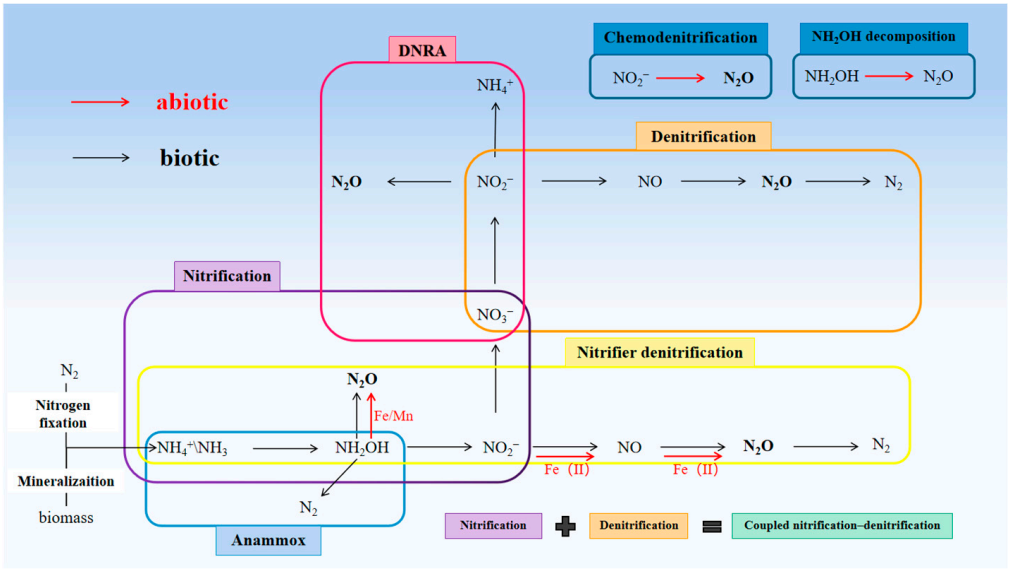

Figure 3. Schematic diagram of biological and abiotic pathways of N_2O production.

2.2. Abiotic Pathways

Since the intermediates (NH_2OH and NO_2^-) of microbial nitrification and denitrification are highly chemically reactive, they are quickly chemically converted into N_2O when leached into the environment [54]. Under acidic conditions, NO_2^- is protonated to HNO_2, which is more reactive than NO_2^- and easily reduced to N_2O by soil organic matter or reduced transitional metals in the environment [55]. The chemical pathway in which NO_2^- is chemically reduced to N_2O is called chemodenitrification (Equations (1) and (2)). Ferrous iron (Fe (II)) and lignin-derived soil organic compounds are common reductants in chemodenitrification [44,56–60]. In general, structural iron plays a more important role in chemodenitrification compared with dissolved free Fe (II) ions [61]. In contrast to chemodenitrification, the chemical oxidation of NH_2OH becomes quicker when the pH increases because NH_2OH is more stable in acidic conditions [54]. When NH_2OH is leached into the environment, it can be easily oxidized to N_2O by oxidative transition metals, such as Fe (III) and Mn^{4+} (Equations (3) and (4)).

$$4Fe^{2+} + 2NO_2^- + 5H_2O \rightarrow 2Fe^{3+} + N_2O + 6H^+ \quad (1)$$

$$2Mn^{2+} + 2NO_2^- + 6H^+ \rightarrow 2Mn^{4+} + N_2O + 3H_2O \quad (2)$$

$$4Fe^{3+} + 2NH_2OH \rightarrow 4Fe^{2+} + N_2O + H_2O + 4H^+ \quad (3)$$

$$2Mn^{4+} + 2NH_2OH \rightarrow 2Mn^{2+} + N_2O + H_2O + 4H^+ \quad (4)$$

More and more studies demonstrate that chemodenitrification and chemical hydroxylamine oxidation play a significant role in global N_2O production [45,62,63]. At least 15–25% of N_2O formation in coastal marine sediments is caused by chemodenitrification [44]. In the reaction of Fe (II) with NO_2^-, the percentage of NO_2^- converted to N_2O ranges from 11% to 52%, reflecting a considerable difference in the degree of chemodenitrification reactions [56]. In intertidal sediments, N_2O production with NO_2^- as a precursor averaged from 70% to 80%, indicating that the N_2O was largely catalyzed by fungal denitrification and abiotic reactions such as chemodenitrification [59]. Abiotic NH_2OH oxidation is also an important

source of N_2O in coastal ecosystems; it has been reported that NH_2OH produced by nitrifying bacteria is rapidly oxidized to N_2O by active Mn (III/IV)-oxidizing minerals [64]. It has been proved that abiotic N_2O production plays an important role in coastal N_2O emissions, while their roles in streams and seawater are still unclear [37,44,59,64,65].

3. Assessment of Aquatic N_2O Budget

3.1. N_2O Flux Measurements

Floating chambers, including static and dynamic floating chambers, are the most commonly used methods to determine the spatiotemporal variation in aquatic N_2O emissions [66]. The floating static chamber refers to using a top-sealed box placed on the surface of the water to collect the N_2O emitted from the surface water through diffusion (Figure 4a). The N_2O concentration in the chamber will be analyzed at regular time intervals in the laboratory [67,68], so that the N_2O fluxes can be calculated according to the increasing rate of N_2O concentration in the chamber over time, as follows [67–70]:

$$F_{N2O} = \frac{n_t - n_0}{A \times t} \quad (5)$$

where F_{N2O} (mol m^{-2} d^{-1}) is the N_2O flux through the water–air interface; n_t (mol) and n_0 (mol) are the mole numbers of N_2O in the chamber at time t and 0, respectively; A (m^2) is the surface area of the chamber in contact with water; and t (day) is the time for which the concentration of the gas increases linearly.

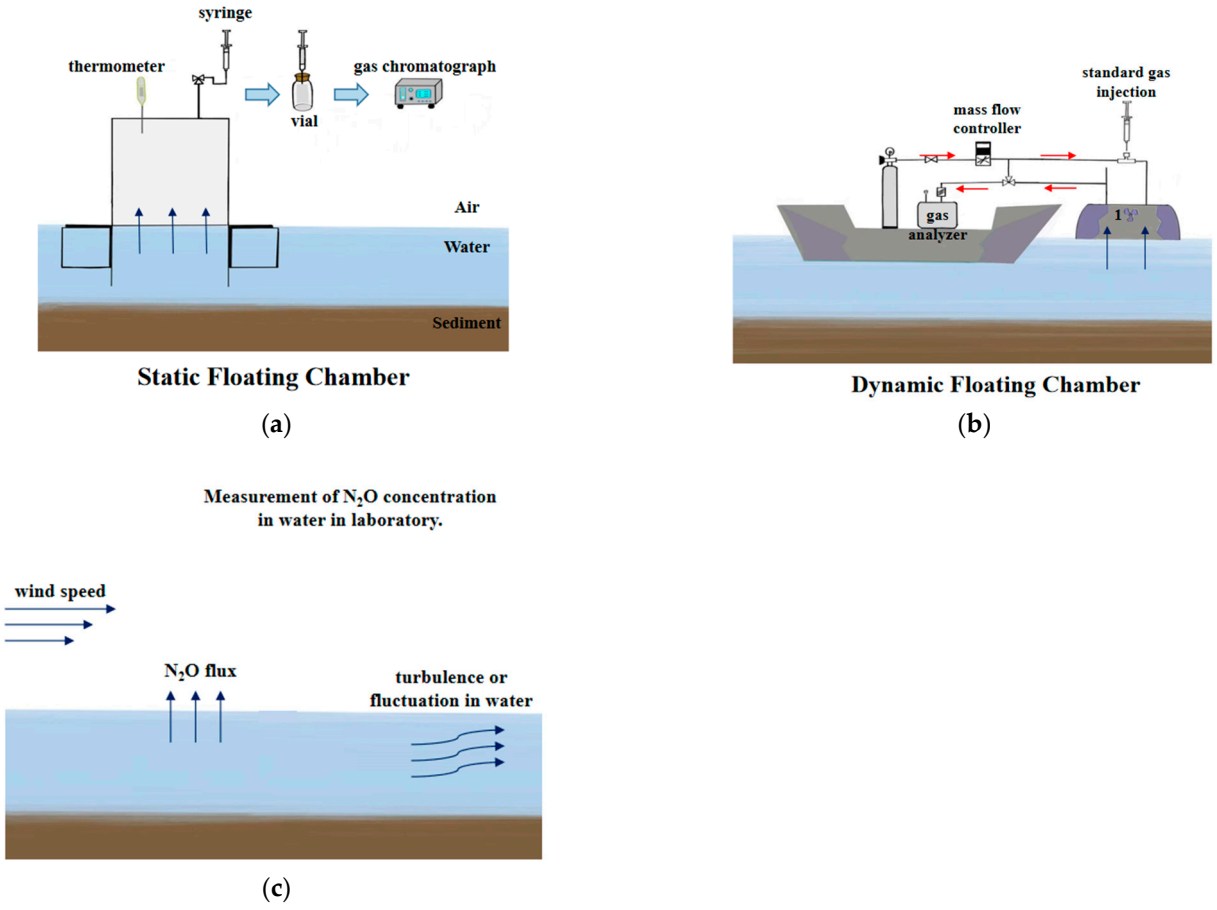

Figure 4. Diagram of N_2O flux measurement with static floating chamber (**a**), dynamic floating chamber (**b**), and water–air gas exchange model (**c**). The red arrow in Figure (**b**) represents the direction of the gas flow in the carrier pipe, and the "1" represents the electric fan in the chamber, which allows the gas to flow.

In contrast, the dynamic floating chambers are based on continuous measurements of gases in the chamber (Figure 4b) [66,71]. At a given airflow rate, the dynamic chamber can reach a steady state in a short time after placement and it can reduce headspace concentration build-up in the gas chamber [66,72]. The gas flow rate extracted by the gas analyzer is about 0.52 L min^{-1}, which is lower than the flow rate of N_2-loaded gas controlled by the mass flow controller (7.72L min^{-1}) [66]. In addition, an injection port is added to the intake carrier pipe (near the syringe in Figure 4b), which can be used to inject a known volume of greenhouse gases for calibration. In terms of ebullitive fluxes, the method can detect bubbles containing more than 1.6×10^{-3} mL of gas and a larger chamber surface area in contact with water will improve the ability to trap more bubbles in a given time [66]. It has been found that continuous monitoring data can accurately reflect the 24 h N_2O emission concentration [71]. The flux can be determined by following equation [66]:

$$F = \left(\frac{d\left(\theta\frac{dC_D}{dt} + C_D\right)}{dt} + \frac{\theta_D\frac{dC_D}{dt} + C_D - C_0}{\theta_{DC}}\right) \times \frac{V_{DC}}{A_{DC}} \quad (6)$$

where F indicates the instantaneous flux (g m^{-2} s^{-1}); C_D is the N_2O concentration (g m^{-3}) measured by the gas analyzer; C_0 is the potential concentration of the influent gas (g m^{-3}); θ_{DC} and θ_D are the residence time (s) in the dynamic chamber and the cavity of the gas analyzer, respectively; V_{DC} is the volume (m^3) of the headspace of the dynamic chamber; and A_{DC} is the area (m^2) of the dynamic chamber in contact with the aquatic ecosystem.

The uncertainty of static floating chamber methods mainly comes from the natural turbulence at the water–air interface when deploying floating chambers, so this method is recommended for low fraction and low wave conditions [10,20]. The impact of natural turbulence can be reduced by minimizing the chamber size, smoothing the surface, employing calm water conditions, and taking measurements during stable meteorological conditions. The gas detection accuracy of a dynamic floating chamber is affected by the carrier gas flow and the surface water area covered by the floating chamber. Therefore, it is necessary to set appropriate experimental parameters and select a detector with high sensitivity. For example, the internal pump of the ultra-portable greenhouse gas analyzer (UGGA, Model 915-0011, Los Gatos Research, Inc., Mountain View, CA, USA) can be used to extract the gas in the chamber and determine the concentration of greenhouse gases and water vapor at 1hz [66].

The water–air gas exchange model is another method to indirectly estimate the aquatic N_2O flux (Figure 4c) [73]. It is based on the principle that the gas transfer at the water–air interface depends on the combination of the gas diffusion rate and concentration gradient [74]. The gas exchange model aims to calculate the N_2O flux (F_{N2O}) according to the N_2O water–air gas transfer velocity (k_w) using the following formulas [15,42,67,75–77]:

$$F_{N2O} = k_w\left(C_{obc} - C_{eq}\right) \quad (7)$$

$$k_w = k_{600}\left(\frac{S_c}{600}\right)^{-0.5} \quad (8)$$

$$S_c = 2055.6 - 137.11t + 4.3173 \times t^2 - 0.054350 \times t^3 \quad (9)$$

where F_{N2O} and k_w are in the units of μmol·m^{-2}·d^{-1} and m·d^{-1}, respectively; C_{obs} is the measured concentration (μmol L^{-1}) of dissolved N_2O in the water, C_{eq} (μmol L^{-1}) represents the air-equilibrated concentration of dissolved N_2O, which is calculated according to the temperature, air pressure, and salinity of the sampling sites; S_c is the Schmidt coefficient in fresh water; and t refers to the in situ temperature. k_{600} is the normalized value to a Schmidt coefficient of 600 at 20 °C, which is generally calculated by empirical hydrology parameter models.

The uncertainties of the water–air gas exchange method are associated with how the wind or water turbulence flow affects gas exchange across the water–air interface [10]. Several different equations for k_{600} can be used to calculate a series of fluxes to reduce the deviation [15,20]. Equations that include the slope and velocity of a river are the best at predicting the speed of gas transfer, while equations that include depth terms have the strongest correlations (Table 1) [78], and other wind-speed-based or wind speed–hydrological models also used to calculate k_{600} (Table 1). The gas flux calculated using the multi-model average k_{600} is conservative but comparable to other models [15]. Field measurements of N_2O obtained from the above bottom-up methods are often used to estimate N_2O emissions in regional and global aquatic ecosystems but basically show high spatiotemporal heterogeneity [10,79].

Table 1. Equations for predicting the k_{600} (m d^{-1}) based on stream velocity (V, in m s^{-1}), slope (S, unitless), depth (D, in meters), discharge (Q, in m^3 s^{-1}), the Froude number ($Fr = V/(gD)^{0.5}$), and wind speed at a 10 m height (W, in m s^{-1}). All p-values for the regressions are 0.001. "-" indicates no measurement.

Model Equation	R^2	Slope	y-Intercept	Ref.
$k_{600} = (VS)^{0.89} \times D^{0.54} \times 5037$	0.72	0.92 ± 0.024	0.98 ± 0.17	
$k_{600} = 5937 \times (1–2.54 \times Fr^2) \times (VS)^{0.89} \times D^{0.58}$	0.76	0.94 ± 0.022	0.76 ± 0.16	
$k_{600} = 1162 \times V^{0.85} S^{0.77}$	0.54	0.91 ± 0.036	0.91 ± 0.24	
$k_{600} = (VS)^{0.76} \times 951.5$	0.53	0.82 ± 0.037	0.92 ± 0.24	[8]
$k_{600} = VS \times 2841 + 2.02$	0.55	1.0 ± 0.038	-4.8×10^{-3} ± 0.26	
$k_{600} = 929 \times (VS)^{0.75} \times Q^{0.011}$	0.53	0.92 ± 0.036	0.81 ± 0.24	
$k_{600} = 4725 \times (VS)^{0.86} \times D^{0.66} \times Q^{-0.14}$	0.76	0.95 ± 0.023	0.57 ± 0.17	
$k_{600} = 1.91 \times e^{0.35W}$	-	-	-	[80]
$k_{600} = 0.314 \times W^2 - 0.436 \times W + 3.99$	-	-	-	[81]
$k_{600} = 1.0 + 1.719 \times (V/D)^{0.5} + 2.58 \times W$	-	-	-	[82]
$k_{600} = 17.19 \times V^{0.5} \times D^{-0.5} + 2.58 \times W + 1.0$	-	-	-	[83]

3.2. Estimation Based on Emission Factor (EF)

IPCC Tier 1 assumes that the N_2O emissions from aquatic systems can be estimated based on the emission factor (EF) of total N leached into aquatic systems [47,84–87]:

$$\boldsymbol{N_2O{-}N_{emission} = EF \times Total_N} \quad (10)$$

where N_2O-$N_{emission}$, Total N, and EF are in units of kg N_2O-N yr^{-1}, kg N yr^{-1}, and kg N_2O-N kg^{-1} N, respectively [1,85]. The default EF value was set at 0.0075 kg N_2O-N/kg N by IPCC in 1997 and revised down to 0.0025 kg N_2O-N/kg N for the convenient estimation of N_2O emission from rivers [86,88,89]. But this recommendation was later revised to 0.0026 kg N_2O-N/kg NO_3-N for rivers, reservoirs, and down-streams, while the EFs for outer estuaries, coastal seawater, and open ocean are still missing [85,89].

In practical application, the data acquisition of N leaching and runoff required to determine the EF of all aquatic ecosystems based on the IPCC definition is incomplete and difficult [10,90–92]. Therefore, many studies choose to estimate the EF using the actual NO_3^- concentrations in focused aquatic systems [10,89,93,94]:

$$\boldsymbol{EF = \frac{C_{N2O}{-}N}{C_{NO_3^-}{-}N}} \quad (11)$$

where C_{N2O-N} (mg·L^{-1}) and C_{NO3-N} (mg·L^{-1}) are concentrations measured in the water.

Uncertainty may be introduced when using EF-based estimation [42] because it ignores potential differences in spatial and temporal N delivery efficiency [90], and multiple sources of input may result in the supersaturation of N_2O [7,78,95,96]. Moreover, N_2O in aquatic ecosystems is mainly produced and consumed through nitrification

and denitrification pathways, but the EF-based method does not take into account that these processes may differ significantly under different conditions in diverse waters [68,97]. It is suggested that N_2O_N/NH_4^+ should be used to calculate EF in river sections with the ammonium nitrogen pollution type, and N_2O_N/DIN ($DIN \approx NO_3^- + NH_4^+$) should be used to calculate the EF when both NO_3^- and NH_4^+ are considerable N pollutants [98].

Data analysis based on global observations shows that the N_2O fluxes in rivers are positively correlated with the concentrations of NH_4^+, NO_3^-, and DIN [90]. N_2O concentrations and EF values show spatial differences associated with different land use types along water bodies [89,99]. The values of EFs could range from 0.000028 to 0.022, corresponding to the variability in the regional environmental condition (Table 2). The concentrations of dissolved N_2O and NO_3^- were usually higher in agricultural and urban rivers [89]. N_2O flux may be determined by NH_4^+ concentration in some urban river networks, while NO_3^- plays a more important role in agricultural watersheds [42,67,100,101]. For example, in the Liaohe River basin in northeast China, sewage and aquaculture wastewater discharge leads to NH_4^+ (0.2–15.5mg/L) pollution in the river, while those polluted by NO_3^- (0.02–9.6mg/L) are mainly distributed in agricultural areas, and the EFs are 0.4456 and 0.0005, respectively [98]. Therefore, the EFs for inland waters and estuaries should fully consider the influence of specific factors such as river basin land use type and water pollution type, and adopting region-specific EF values is more appropriate for the estimation of regional and global aquatic N_2O emissions [10,89,102].

Table 2. N_2O fluxes and EFs of different rivers.

Regions	Aquatic Ecosystems	N_2O Flux ($\mu mol \cdot m^{-2} \cdot d^{-1}$)	NH_4^+ (mg/L)	NO_3^- (mg/L)	EFs (%)	Ref.
Southeast China	Min River Basin	−0.84–3.12	0.01–2.3	1.9–11.9	0.043–0.93 [a]	[103]
	Estuary of Min River	−2.9–4.3	0.01–0.2	0.4–2.7	0.029–0.25 [a]	[104]
Northeast China	Liao River Basin	9.36–8539.2	0. 2–15.5	0.02–9.6	0.01–2.2 [b]	[98]
	Daliao River and Estuary	4.6–145.1	-	-	-	[105]
	Lower Haihe River Basin	−7.2–160.8	0.1–0.2	0.3–0.5	0.20–0.39 [a]	[106]
North China	Beitang Drainage River and Dagu Drainage River	44.6 ± 39.4	3.3–10.6	-	0.007–0.1 [b]	[107]
	Duliujian River, Yongdingxin River, and Nanyuhe River	26.9 ± 31.2	3.3–10.6	-	0.003–0.09 [b]	[107]
Eastern China	Middle and lower reaches of the Yangtze River	0.1–35.0	0.2–0.3	2.6–6.9	0.033–0.053 [a]	[22]
	Chaohu River Basin	0.4–2102.6	0.3–12.5	0.5–0.7	0.027–0.80 [a]	[88]
	Xin'an Tang River in Taihu region	35.3–86.7	0.5–1.2	3.0–7.2	0.040–0.044 [a]	[108]
Southwest China	Chongqing metropolitan river network	4.5–1566.8	-	3.7 ± 2.5	0.47 [a]	[99]
	Qingshui Stream, Taohua Stream, Panxi Stream, Xiaojia River, Fenghuang Stream, and Jiuqu River in Chongqing	10–4940	0.1–1.6	1.1–9.6	0.14–0.29 [a]	[15]
	Lancang River	7.70–26.00	0.18–0.45	0.26–0.53	0.41–0.61 [a]	[109]
Western China	The upper reaches of Yangtze River, Yellow River, Lancang River, and Nu River	9.4 ± 6.2	-	-	0.1 [a]	[68]
South China	Shenzhen River, Dashahe River, Xixiang River	-	0–9.6	0.3–15.8	0.0028–0.44 [a]	[110]
	Estuary of Pearl River	31.9 ± 7.5	-	-	-	[76]
		37 ± 15	0–8.46	0–14.26	0.13 [a]	[111]

Table 2. *Cont.*

Regions	Aquatic Ecosystems	N_2O Flux ($\mu mol \cdot m^{-2} \cdot d^{-1}$)	NH_4^+ (mg/L)	NO_3^- (mg/L)	EFs (%)	Ref.
USA	San Joaquin River	22.6–177.4	-	0.2–15.5	0.003–0.21 [a]	[67]
	Kalamazoo River	−7.7–228.7	0–0.4	0.003–27.4	0.05–0.014 [a]	[42]
	Connecticut River	28.9	0.03–0.07	0.5–2.3	0.09–0.44 [a]	[84]
Canada	Grand River	−35–4200	-	-	-	[68]
	Ontario Streams	0.48–199.2	0.002–0.4	0.5–12.8	-	[101]
Sweden	Uppsala watershed	92.5–150	<0.1	4.4–22.1	0.11 [a]	[100]
Japan	Tama River	-	0.4–0.7	8.0–30.9	0.019 [a]	[94]
France	Haut-Loir watershed	-	0.03–0.05	27.9–50.5	0.014–0.095 [a]	[112]
	Seine River	2.3–193.2	-	22.1–31	0.01–0.028 [a]	[95]
Sub-Saharan Africa	Congo River	−52–319	0.04	0.4	0.0024 [a]	[113]
Kenya	Mara River	13.7	0.02–0.19	0.65–1.77	0.031–0.04 [a]	[114]
Malaysia	Lupar and Saribas Rivers	21.3	0.012–0.12	0.3–2.3	0.1–1.19 [a]	[48]
South Asia	Cochin Estuary	0.5–29.7	0.02–0.5	0.4–2.6	0.21–0.37 [a]	[115]
	Adyar River and Estuary	0.24–122.4	7.6–77	0.3–2.8	0.03–1.76 [a]	[116]
UK	Upper Thurne River	129.8	0.4	7.1	0.11 [a]	[91]
	Wensum, Eden, and Avon Rivers	50.0	-	19.8–37.7	0.006–0.24 [a]	[102]
New Zealand	LII River	20.6–273.4	-	11.1–23.5	0.023–0.048 [a]	[75]
	Ashburton River	8.6–16.3	-	0.09–6.02	0.17–1.69 [a]	[117]

[a] The N_2O concentration in water divided by the NO_3^- concentration. [b] The N_2O concentration in water divided by the concentration of NO_3^- and NH_4^+. "-" indicates no measurement.

3.3. Model Simulation

The modeling of N_2O emissions from aquatic ecosystems can be mainly categorized into two types: statistical models and process-based models. Statistical models of N_2O emissions, including empirical models and semi-empirical models, rely on multiple linear regression analysis which can reflect statistical relationships between emission data and their controlling factors [7,31,118–120]. For example, the global Nutrient Export from WaterShed (NEWS) model is the first global applicable semi-empirical model used to estimate aquatic N load rates and N_2O emissions [47,119]. The model estimates N load rates as a function of human activities, such as nitrogen fertilizer use, human sewage, and atmospheric nitrogen deposition [31]. The estimated global N_2O emission from rivers and estuaries based on this model is 1.32 Tg N yr^{-1} [119]. The global ocean N_2O emissions are estimated to be 2.45 ± 0.80 Tg N yr^{-1} by a semi-empirical model based on the relationship between ocean primary productivity and the N cycle [30]. Machine learning algorithms, such as Random Forest or Monte Carlo simulation, can be used to identify complex relationships between multiple variables [9,10,26].

Process-based models for N_2O emissions are based on the biogeochemical and physical processes that drive N_2O emissions. For example, the Dynamic Land Ecosystem Model (DLEM) riverine module simulates N_2O emissions according to nitrification and denitrification rates, N inputs, N retention and release rates, oxygen consumption, and organic matter decomposition and estimated riverine N_2O emission to be 0.3 ± 0.06Tg N yr^{-1} [14]. The Bern3D Earth system model calculates N_2O emissions based on denitrification and organic matter consumption and estimates an oceanic N_2O budget of 4.5 ± 1.0 Tg N yr^{-1} [25]. Process-based models show good advantages to estimate aquatic N_2O emissions in the absence of measured data and to predict the response of N_2O fluxes to multifactor climate and environmental changes [25,79,121,122]. In addition, the process-based N_2O emission model can be integrated with hydrological models to predict changes in N_2O emissions in response to land use changes beside the water bodies [37,118,123].

Even though multiple models have been developed to predict aquatic N_2O emissions, their results vary from model to model, regarding both natural and anthropogenic sources. The total N_2O emission in rivers and oceans ranges largely from 0.03 to 1.05 Tg N yr^{-1} and from 2.45 to 4.50 Tg N yr^{-1}, respectively (Table 3). The uncertainties of N_2O-predicting models mainly come from the fact that (1) measurement data are highly limited due to the difficulties of field sampling and (2) the mechanisms involved in aquatic N_2O emissions are not yet fully interpreted [47].

Table 3. Estimates of global aquatic emissions of N_2O by different models or methods in units of Tg N yr^{-1}. "-" indicates no measurement.

N_2O Emission	Natural	Anthropogenic	Total	Models/Methods	Ref.
Global	9.7 (8.0–12.0)	7.3 (4.2–11.4)	17	Process-based model (DLEM)	[79]
Inland and coastal waters	0.3 (0.3–0.4)	0.5 (0.2–0.7)	0.8	Process-based model (DLEM)	[79]
Rivers and estuaries	0.07	1.25	1.32	Semi-empirical model (NEWS)	[23]
Continental shelves	0.5	0.1	0.6	Semi-empirical model (NEWS)	[23]
Estuaries	-	-	0.148–0.277	Process-based N balance model	[120]
Rivers, reservoirs, lakes, ponds, streams	-	-	0.94	Empirical Monte Carlo simulation	[10]
Estuaries	-	-	0.26	Empirical Monte Carlo simulation	[10]
Riverine	-	-	0.3 ± 0.06	Process-based model (DLEM)	[14]
Riverine	-	-	0.073	Semi-empirical model	[9]
Riverine	-	-	0.03–0.035	Empirical multiple regression model	[90]
Riverine	0.105	0.945	1.05	Semi-empirical model (NEWS)	[124]
Oceans	3.4 (2.5–4.3)	0.1 (0.1–0.2)	3.5	Process-based model (DLEM)	[79]
Oceans	4.2 ± 1.0	-	4.2 ± 1.0	Empirical Random Forest model	[26]
Oceans	-	-	4.5 ± 1.0	Bern3D Earth System model	[25]
Oceans	-	-	2.45± 0.8	Semi-empirical N cycle model	[30]
Oceans	3.5	0	3.5	Semi-empirical model (NEWS)	[23]

3.4. Uncertainties

Most N_2O emission inventories rely on simple EF methods or model studies [47]. Field measurements provide the most realistic estimates of N_2O fluxes and can provide spatiotemporal datasets for model calibration and verification [10,37,96]. While more field measurements can yield more accurate EFs, they also bring uncertainty due to aquatic conditions and the heterogeneity in land use types along water bodies, leading to a wide range of N_2O estimations [14,90,120,125–127]. Moreover, the large-scale deployment of EF measurements is difficult and labor-intensive, and the assessment of aquatic ecosystem EFs using the IPCC method needs detailed N-relevant data, which are difficult to obtain and often missing in many studies [37,70,127]. Despite the limitations, field measurements play an important role in providing accurate estimates of N_2O fluxes and improving model frameworks. In the future, it is necessary to take into

account river hydrological characteristics and measure more data for the revision of IPCC EFs [67,125].

There is considerable uncertainty in the assessment of N_2O emission models at both regional and global scales [7,9,118,120]. Uncertainties come mainly from the complexity of the aquatic ecosystems and inadequate measurement data [123,128]. More data networks need to be established to improve model prediction and validation performance [25,28,79]. The N_2O model comparison project is proposed to better identify and ultimately reduce these uncertainties between different models [121], and additional long-term studies measuring results in aquatic ecosystems are needed [28,47].

4. N_2O Source Partitioning with Stable Isotope Technique

4.1. Stable Isotopes of N_2O

Isotopes are atoms of the same element that have different numbers of neutrons, resulting in different atomic masses, such as ^{14}N and ^{15}N and ^{16}O and ^{18}O. The stable isotope technique is widely used in the qualitative measurement of N-transforming processes, and it is also an effective method to study the pathway of N_2O production [36]. N_2O is an asymmetric linear molecule with the proximal and distal N of the O atom called N^{α} and N^{β}, respectively. The difference in ^{15}N enrichment of N^{α} and N^{β} is defined as site preference (SP) of N_2O [4]:

$$\delta^{15}N^{bulk} = \frac{\left(\delta^{15}N^{\alpha} + \delta^{15}N^{\beta}\right)}{2} \quad (12)$$

$$SP = \delta^{15}N^{\alpha} - \delta^{15}N^{\beta} \quad (13)$$

where $\delta^{15}N^{\alpha}$ and $\delta^{15}N^{\beta}$ denote the relative ^{15}N abundance of N^{α} and N^{β}, respectively.

Isotopes substituted by ^{15}N or ^{18}O are usually studied to provide information about the formation and decomposition processes of N_2O [129,130].

Obvious differences in $\delta^{15}N$ and SP values were detected among each aquatic ecosystem (Figure 2). The $\delta^{15}N$-N_2O values of freshwater and seawater are $-4.64 \pm 9.84‰$ and $6.63 \pm 3.50‰$, respectively [34]. The isotopic characteristics of N_2O are controlled by biological, chemical, and physical fractionations, as well as isotopic characteristics of N substrates [101]. Due to the isotope fractionation effect of each N_2O production pathway, the stable isotopic values can be used to analyze the relative contributions of the N_2O production pathways [43,57].

4.2. Isotopic Characteristics of Biological Processes

During nitrification, the isotope effect of N_2O production ($\delta^{15}N$-N_2O) by the oxidation of NH_4^+ is $-56.6 \pm 7.3‰$, but when NH_2OH is the only substrate, the $\delta^{15}N$-N_2O increases to $-5.1 \pm 12.0‰$ [131]. In aquatic environments, the isotope effect of NO_3^- reduced to NO_2^- is $-14.3 \pm 9.7‰$, while the $\delta^{15}N$-N_2O for denitrification and nitrifier denitrification from NO_2^- to N_2O can be represented by $-14.9 \pm 6.7‰$ and $-34.5 \pm 0.7‰$, respectively [131,132]. The ranges of $\delta^{18}O$-N_2O produced by fungal denitrification and NH_4^+ by bacterial nitrification are between 27‰ and 42‰ and 20‰ and 26‰, respectively. The $\delta^{18}O$-N_2O difference is partly due to the different isotopic compositions of O-containing sources. In the process by which bacteria produce N_2O by oxidizing NH_4^+, the O comes from oxygen and water vapor in the atmosphere. On the contrary, oxygen atoms are derived from NO_3^- or NO_2^- substrates during denitrification [133].

Tracing the path of N_2O production by using these SP values has become a research hotspot [6,41,132,134]. The SP values of N_2O produced by different paths have certain differences, ranging from −11‰ to 36.9‰ (Tables 4 and 5). Unlike $\delta^{18}O$ and $\delta^{15}N$, SP is thought to reflect the N_2O production mechanism while remaining independent of the

substrate's isotopic signature [135]. For example, when nitrifying bacteria produce N_2O, there may be a positive correlation between SP and $\delta^{18}O$-N_2O, resulting from nitrification by mixing high SP and ^{18}O-enriched N_2O from hydroxylamine decomposition with low SP and ^{18}O-depleted N_2O from nitrifying denitrification [43]. Compared with aerobic denitrification and bacterial denitrification, the N_2O process produced by fungal denitrification and nitrification has a higher SP value [36,136]. The SP value of the coupled nitrification and denitrification process is similar to that of denitrification, with a value of 0.1 ± 1.7‰, indicating that the isotopic SP value can distinguish nitrification from coupled nitrification and denitrification [132]. In addition, differences in the experimental environment or the presence of an unknown N_2O production pathway in the sample will influence the measurement of the SP value. Therefore, it is necessary to reduce uncertainties and limitations through more experiments in the future.

4.3. Isotopic Characteristics of Abiotic Processes

Dual isotope ecosystems of N and O have also made further progress in their application to distinguish abiotic processes. The SP reflects the difference in the regulatory reaction mechanism, and the end value is related to the final concentration and yield of N_2O [56]. For the abiotic reduction of NO_2^- by Fe (II), the $\delta^{15}N$ and $\delta^{18}O$ of N_2O ranges from −19.8‰ to −3.0‰ and from 29.3‰ to 46.4‰, respectively [56]. The SP values of N_2O produced by NH_2OH oxidation and NO_2^- reduction processes are 30.1‰ and 29.5‰, respectively [135], while in the process of NO_2^- reduction catalyzed by Fe (II), the SP value ranges from 0.4‰ to 35‰ [56,57,137]. In addition, the reported SP of chemodenitrification ranges from −4‰ to 26.5‰, which overlaps with the SP value of biological processes [45,56,57,61]. At present, although the SP value is an important indicator to identify the pathways of N_2O production, most of the studies are pure culture experiments conducted in the laboratory [56,57,61], and the differentiation characteristics of N and O isotope effects on N_2O produced by the coupling of NH_2OH and NO_2^- with Fe/Mn in various natural aquatic environments remain unclear, which limits the understanding of the mechanism of N_2O production.

Table 4. Summary of N_2O isotope characteristics produced by each pathway.

N_2O Sources	Reaction Type	$\delta^{15}N$-N_2O (‰)	$\delta^{18}O$-N_2O (‰)	SP (‰)	Ref.
Ocean	-	8.8	60.7	35.7	[138]
	-	−6~21	-	-	[139]
	Biotic	3.5~5.5	35.5~41.5	0–8	[33]
Natural or agricultural soil	Biotic	−38~6	-	-	[139]
Antarctic soil	Biotic + Abiotic	−82 ± 1	23 ± 1	22 ± 1	[62]
11 rivers in southern Ontario, Canada	-	−22.6~10.7	47.4~51.5	-	[101]
Estuarine salt marsh	Biotic	−1.41~2.99	39.66~50.38	4.09~13.69	[129]
Troposphere	-	7.0 ± 0.6	43.7 ± 0.9	18.7 ± 2.2	
Stratosphere	-	11.4	48.3	21.3	[140]
Weighted average of marine and land sources	Biotic + Abiotic	−25.5~1.0	9.8~37.4	−0.5 ~15.1	

"-" indicates no measurement.

Table 5. Summary of N_2O isotope characterization of biotic and abiotic processes.

Reaction Process	N_2O Sources	$\delta^{15}N$-N_2O (‰)	$\delta^{18}O$-N_2O (‰)	SP (‰)	Ref.
Biotic	Oxidation of NH_2OH and $NH4^+$	-	-	32~35	[132]
	Denitrification of NO_2^- and NO_3^-	-	-	0	
	NO_2^- reduction	−90~2	13~35	−11~0	[6]
	NH_2OH oxidation	-	−10	-	[41]
		−68~19	22~24.5	13~37	[6]
		-	-	32.5~35.6	[132]
	Nitrification	-5.1 ± 12.0	-	-	[131]
		-56.6 ± 7.3	-	-	[131]
	Bacterial denitrification	-	-	23.3 ± 4.2, -5.1 ± 1.8	[134]
	Fungal denitrification	-	37.3 ± 1.3, 31.5 ± 0.5	37.1 ± 2.5, 36.9 ± 2.8	[133]
		-	-	15.8~36.7	[52]
Abiotic	Nitrifier denitrification	-	-	0.1 ± 1.7	[132]
	NO_2^- reduction	-	-	30.1 ± 1.7	[134]
	NH_2OH oxidation	-	-	29.5 ± 1.1	[134]
	Chemodenitrification	2~11	4~10	26.5 ± 0.8	[61]
		−19.8~−3.0	29.3~46.4	0.4~26.0	[56]
		-	-	10~22	[57]

"-" indicates no measurement.

5. Research Prospect

Aquatic ecosystems are important global N_2O sources, but uncertainties still exist in the quantification of the aquatic N_2O budget. To understand more precisely the aquatic N_2O emissions, further studies should be conducted to (1) establish more N_2O flux measurements in aquatic ecosystems, especially data-inadequate areas such as oceans and arctic regions; (2) interpret more clearly the mechanisms involved in aquatic N_2O production and its controlling environmental factors; (3) decrease the uncertainties of N_2O-predicting models and make the results of different models more comparable; and (4) advance the application of stable isotopic techniques in aquatic N_2O emissions regarding both mechanism studies and model establishment.

Author Contributions: Methodology, H.P. and J.W.; Validation, H.P., Z.Z. and S.Z.; Investigation, H.P., Z.Z., S.Z. and F.W.; Data curation, H.P.; Writing—original draft, H.P. and J.W. All authors have read and agreed to the published version of the manuscript.

Funding: This study was supported by the Guangdong Major Project of Basic and Applied Basic Research (2020B0301030004), the National Natural Science Foundation of China (Nos. U21A6001; 42203004), Innovation Group Project of Southern Marine Science and Engineering Guangdong Laboratory (Zhuhai) (No. 311021009), and the Guangdong Provincial Department of Science and Technology (2019ZT08G090).

Data Availability Statement: Data is available under request.

Conflicts of Interest: The authors declare no conflict of interest.

References

1. IPCC. Global Carbon and other Biogeochemical Cycles and Feedbacks. In *Climate Change 2021: The Physical Science Basis. Contribution of Working Group I to the Sixth Assessment Report of the Intergovernmental Panel on Climate Change*; Cambridge University Press: Cambridge, UK; New York, NY, USA, 2021; pp. 673–816. [CrossRef]
2. Basso, L.; Crotwell, A.; Dolman, H.; Gatti, L.; Gerbig, C.; Griffith, D.; Hall, B.; Jordan, A.; Krummel, P.; Loh, Z.; et al. *WMO Greenhouse Gas Bulletin. The State of Greenhouse Gases in the Atmosphere Based on Global Observations through 2020*; World Meteorological Organization: Geneva, Switzerland, 2021.
3. Bange, H.W.; Rapsomanikis, S.; Andreae, M.O. Nitrous oxide in coastal waters. *Glob. Biogeochem. Cycles* **1996**, *10*, 197–207. [CrossRef]
4. Pauleta, S.R.; Carepo, M.S.P.; Moura, I. Source and reduction of nitrous oxide. *Coord. Chem. Rev.* **2019**, *387*, 436–449. [CrossRef]

5. Ravishankara, A.R.; Daniel, J.S.; Portmann, R.W. Nitrous oxide (N_2O): The dominant ozone-depleting substance emitted in the 21st century. *Science* **2009**, *326*, 123–125. [CrossRef] [PubMed]
6. Humbert, G.; Sébilo, M.; Fiat, J.; Lang, L.; Filali, A.; Vaury, V.; Spérandio, M.; Laverman, A.M. Isotopic evidence for alteration of nitrous oxide emissions and producing pathways contribution under nitrifying conditions. *Biogeosciences* **2019**, *17*, 979–993. [CrossRef]
7. Beaulieu, J.J.; Tank, J.L.; Hamilton, S.K.; Wollheim, W.M.; Hall, R.O., Jr.; Mulholland, P.J.; Peterson, B.J.; Ashkenas, L.R.; Cooper, L.W.; Dahm, C.N.; et al. Nitrous oxide emission from denitrification in stream and river networks. *Proc. Natl. Acad. Sci. USA* **2011**, *108*, 214–219. [CrossRef] [PubMed]
8. Raymond, P.A.; Zappa, C.J.; Mulholland, P.; Laursen, A.E.; Butman, D.; Bott, T.L.; Potter, J.; McDowell, W.H.; Newbold, D. Scaling the gas transfer velocity and hydraulic geometry in streams and small rivers. *Limnol. Oceanogr. Fluids Environ.* **2012**, *2*, 41–53. [CrossRef]
9. Marzadri, A.; Amatulli, G.; Tonina, D.; Bellin, A.; Shen, L.Q.; Allen, G.H.; Raymond, P.A. Global riverine nitrous oxide emissions: The role of small streams and large rivers. *Sci. Total Environ.* **2021**, *776*, 145148. [CrossRef] [PubMed]
10. Zheng, Y.; Wu, S.; Xiao, S.; Yu, K.; Fang, X.; Xia, L.; Wang, J.; Liu, S.; Freeman, C.; Zou, J. Global methane and nitrous oxide emissions from inland waters and estuaries. *Glob. Chang. Biol.* **2022**, *28*, 4713–4725. [CrossRef]
11. Gruber, N.; Galloway, J.N. An Earth-system perspective of the global nitrogen cycle. *Nature* **2008**, *451*, 293–296. [CrossRef]
12. Menegat, S.; Ledo, A.; Tirado, R. Greenhouse gas emissions from global production and use of nitrogen synthetic fertilisers in agriculture. *Sci. Rep.* **2022**, *12*, 14490. [CrossRef]
13. Harris, E.; Yu, L.; Wang, Y.P.; Mohn, J.; Henne, S.; Bai, E.; Barthel, M.; Bauters, M.; Boeckx, P.; Dorich, C.; et al. Warming and redistribution of nitrogen inputs drive an increase in terrestrial nitrous oxide emission factor. *Nat. Commun.* **2022**, *13*, 4310. [CrossRef] [PubMed]
14. Yao, Y.; Tian, H.; Shi, H.; Pan, S.; Xu, R.; Pan, N.; Canadell, J.G. Increased global nitrous oxide emissions from streams and rivers in the Anthropocene. *Nat. Clim. Chang.* **2020**, *10*, 138–142. [CrossRef]
15. Wang, X.; Yu, L.; Liu, T.; He, Y.; Wu, S.; Chen, H.; Yuan, X.; Wang, J.; Li, X.; Li, H.; et al. Methane and nitrous oxide concentrations and fluxes from heavily polluted urban streams: Comprehensive influence of pollution and restoration. *Environ. Pollut.* **2022**, *313*, 120098. [CrossRef] [PubMed]
16. Seitzinger, S.; Harrison, J.A.; Böhlke, J.K.; Bouwman, A.F.; Lowrance, R.; Peterson, B.; Tobias, C.; Drecht, G.V. Denitrification across Landscapes and Waterscapes: A Synthesis. *Ecol. Appl.* **2006**, *16*, 2064–2090. [CrossRef] [PubMed]
17. Chen, C.T.A.; Wang, S.L.; Lu, X.X.; Zhang, S.R.; Lui, H.K.; Tseng, H.C.; Wang, B.J.; Huang, H.I. Hydrogeochemistry and greenhouse gases of the Pearl River, its estuary and beyond. *Quat. Int.* **2008**, *186*, 79–90. [CrossRef]
18. Lequy, E.; Asmala, E.; Ibrom, A.; Loubet, B.; Massad, R.S.; Markager, S.; Garnier, J. Contribution from a eutrophic temperate estuary to the landscape flux of nitrous oxide. *Water Res.* **2022**, *222*, 118874. [CrossRef] [PubMed]
19. Zhang, W.X.; Yue, F.J.; Wang, Y.; Li, Y.; Lang, Y.C.; Li, S.L. Dynamic N transport and N_2O emission during rainfall events in the coastal river. *Sci. Total Environ.* **2023**, *23*, 166206. [CrossRef] [PubMed]
20. Murray, R.H.; Erler, D.V.; Eyre, B.D. Nitrous oxide fluxes in estuarine environments: Response to global change. *Glob. Chang. Biol.* **2015**, *21*, 3219–3245. [CrossRef]
21. Wells, N.S.; Maher, D.T.; Erler, D.V.; Hipsey, M.; Rosentreter, J.A.; Eyre, B.D. Estuaries as Sources and Sinks of N_2O Across a Land Use Gradient in Subtropical Australia. *Glob. Biogeochem. Cycles* **2018**, *32*, 877–894. [CrossRef]
22. Yan, W.; Yang, L.; Wang, F.; Wang, J.; Ma, P. Riverine N_2O concentrations, exports to estuary and emissions to atmosphere from the Changjiang River in response to increasing nitrogen loads. *Glob. Biogeochem. Cycles* **2012**, *26*, GB4006. [CrossRef]
23. Seitzinger, S.P.; Kroeze, C.; Styles, R.V. Global distribution of N_2O emissions from aquatic systems: Natural emissions and anthropogenic effects. *Glob. Chang. Sci.* **2000**, *2*, 267–279. [CrossRef]
24. Syakila, A.; Kroeze, C. The global nitrous oxide budget revisited. *Greenh. Gas Meas. Manag.* **2011**, *1*, 17–26. [CrossRef]
25. Battaglia, G.; Joos, F. Marine N_2O Emissions From Nitrification and Denitrification Constrained by Modern Observations and Projected in Multimillennial Global Warming Simulations. *Glob. Biogeochem. Cycles* **2018**, *32*, 92–121. [CrossRef]
26. Yang, S.; Chang, B.X.; Warner, M.J.; Weber, T.S.; Bourbonnais, A.M.; Santoro, A.E.; Kock, A.; Sonnerup, R.E.; Bullister, J.L.; Wilson, S.T.; et al. Global reconstruction reduces the uncertainty of oceanic nitrous oxide emissions and reveals a vigorous seasonal cycle. *Proc. Natl. Acad. Sci. USA* **2020**, *117*, 11954–11960. [CrossRef] [PubMed]
27. Chen, X.; Ma, X.; Gu, X.; Liu, S.; Song, G.; Jin, H.; Zhang, G. Seasonal and spatial variations of N_2O distribution and emission in the East China Sea and South Yellow Sea. *Sci. Total Environ.* **2021**, *775*, 145715. [CrossRef]
28. Bange, H.W.; Arévalo-Martínez, D.L.; de la Paz, M.; Farías, L.; Kaiser, J.; Kock, A.; Law, C.S.; Rees, A.P.; Rehder, G.; Tortell, P.D.; et al. A Harmonized Nitrous Oxide (N_2O) Ocean Observation Network for the 21st Century. *Front. Mar. Sci.* **2019**, *6*, 157. [CrossRef]
29. Leng, P.; Li, Z.; Zhang, Q.; Koschorreck, M.; Li, F.; Qiao, Y.; Xia, J. Deciphering large-scale spatial pattern and modulators of dissolved greenhouse gases (CO_2, CH_4, and N_2O) along the Yangtze River, China. *J. Hydrol.* **2023**, *623*, 129710. [CrossRef]
30. Buitenhuis, E.T.; Suntharalingam, P.; Le Quéré, C. Constraints on global oceanic emissions of N_2O from observations and models. *Biogeosciences* **2018**, *15*, 2161–2175. [CrossRef]

31. Que, Z.; Wang, X.; Liu, T.; Wu, S.; He, Y.; Zhou, T.; Yu, L.; Qing, Z.; Chen, H.; Yuan, X. Watershed land use change indirectly dominated the spatial variations of CH_4 and N_2O emissions from two small suburban rivers. *J. Hydrol.* **2023**, *619*, 129357. [CrossRef]
32. Gao, Y.; Jia, Y.; Yu, G.; He, N.; Zhang, L.; Zhu, B.; Wang, Y. Anthropogenic reactive nitrogen deposition and associated nutrient limitation effect on gross primary productivity in inland water of China. *J. Clean. Prod.* **2019**, *208*, 530–540. [CrossRef]
33. Popp, B.N.; Westley, M.B.; Toyoda, S.; Miwa, T.; Dore, J.E.; Yoshida, N.; Rust, T.M.; Sansone, F.J.; Russ, M.E.; Ostrom, N.E.; et al. Nitrogen and oxygen isotopomeric constraints on the origins and sea-to-air flux of N2O in the oligotrophic subtropical North Pacific gyre. *Glob. Biogeochem. Cycles* **2002**, *16*, 12-1–12-10. [CrossRef]
34. Snider, D.M.; Venkiteswaran, J.J.; Schiff, S.L.; Spoelstra, J. From the ground up: Global nitrous oxide sources are constrained by stable isotope values. *PLoS ONE* **2015**, *10*, e0118954. [CrossRef]
35. Su, X.; Cui, L.; Tang, Y.; Wen, T.; Yang, K.; Wang, Y.; Zhang, J.; Zhu, G.; Yang, X.; Hou, L.; et al. Denitrification and N_2O Emission in Estuarine Sediments in Response to Ocean Acidification: From Process to Mechanism. *Environ. Sci. Technol.* **2022**, *56*, 14828–14839. [CrossRef] [PubMed]
36. Toyoda, S.; Yoshida, N.; Koba, K. Isotopocule analysis of biologically produced nitrous oxide in various environments. *Mass Spectrom. Rev.* **2017**, *36*, 135–160. [CrossRef] [PubMed]
37. Quick, A.M.; Reeder, W.J.; Farrell, T.B.; Tonina, D.; Feris, K.P.; Benner, S.G. Nitrous oxide from streams and rivers: A review of primary biogeochemical pathways and environmental variables. *Earth Sci. Rev.* **2019**, 191. [CrossRef]
38. Thakur, I.S.; Medhi, K. Nitrification and denitrification processes for mitigation of nitrous oxide from waste water treatment plants for biovalorization: Challenges and opportunities. *Bioresour. Technol.* **2019**, *282*, 502–513. [CrossRef] [PubMed]
39. Pandey, C.B.; Kumar, U.; Kaviraj, M.; Minick, K.J.; Mishra, A.K.; Singh, J.S. DNRA: A short-circuit in biological N-cycling to conserve nitrogen in terrestrial ecosystems. *Sci. Total Environ.* **2020**, *738*, 139710. [CrossRef] [PubMed]
40. Wrage-Mönnig, N.; Horn, M.A.; Well, R.; Müller, C.; Velthof, G.; Oenema, O. The role of nitrifier denitrification in the production of nitrous oxide revisited. *Soil Biol. Biochem.* **2018**, *123*, A3–A16. [CrossRef]
41. Baggs, E.M. A review of stable isotope techniques for N_2O source partitioning in soils: Recent progress, remaining challenges and future considerations. *Rapid Commun. Mass Spectrom.* **2008**, *22*, 1664–1672. [CrossRef]
42. Beaulieu, J.J.; Arango, C.P.; Hamilton, S.K.; Tank, J.L. The production and emission of nitrous oxide from headwater streams in the Midwestern United States. *Glob. Chang. Biol.* **2008**, *14*, 878–894. [CrossRef]
43. Frame, C.H.; Casciotti, K.L. Biogeochemical controls and isotopic signatures of nitrous oxide production by a marine ammonia-oxidizing bacterium. *Biogeosciences* **2010**, *7*, 2695–2709. [CrossRef]
44. Otte, J.M.; Blackwell, N.; Ruser, R.; Kappler, A.; Kleindienst, S.; Schmidt, C. N_2O formation by nitrite-induced (chemo)denitrification in coastal marine sediment. *Sci. Rep.* **2019**, *9*, 10691. [CrossRef] [PubMed]
45. Xu, C.; Qi, M.; Lin, W.; Li, X. Nitrous Oxide from Abiotic Processes of Hydroxylamine and Nitrite in Estuarine and Coastal Ecosystems: A Review. *J. Mar. Sci. Eng.* **2022**, *10*, 623. [CrossRef]
46. Deng, W.; Wu, J.; Hong, Y.; Liu, X.; Hu, Y. The diversity distribution and N_2O production driven by fungal denitrification in different natural ecosystems. *Acta Microbiol. Sin.* **2021**, *61*, 1551–1566. (In Chinese) [CrossRef]
47. Ivens, W.P.M.F.; Tysmans, D.J.J.; Kroeze, C.; Löhr, A.J.; van Wijnen, J. Modeling global N_2O emissions from aquatic systems. *Curr. Opin. Environ. Sustain.* **2011**, *3*, 350–358. [CrossRef]
48. Müller, D.; Bange, H.W.; Warneke, T.; Rixen, T.; Müller, M.; Mujahid, A.; Notholt, J. Nitrous oxide and methane in two tropical estuaries in a peat-dominated region of northwestern Borneo. *Biogeosciences* **2016**, *13*, 2415–2428. [CrossRef]
49. Tian, Y.; Yang, P.; Yang, H.; Wang, H.; Zhang, L.; Tong, C.; Lai, D.Y.F.; Lin, Y.; Tan, L.; Hong, Y.; et al. Diffusive nitrous oxide (N_2O) fluxes across the sediment-water-atmosphere interfaces in aquaculture shrimp ponds in a subtropical estuary: Implications for climate warming. *Agric. Ecosyst. Environ.* **2023**, *341*, 108218. [CrossRef]
50. Li, X.; Qi, M.; Gao, D.; Liu, M.; Sardans, J.; Penuelas, J.; Hou, L. Nitrous oxide emissions from subtropical estuaries: Insights for environmental controls and implications. *Water Res.* **2022**, *212*, 118110. [CrossRef]
51. Yang, J.T.; Hsu, T.C.; Tan, E.; Lee, K.; Krom, M.D.; Kang, S.; Dai, M.; Hsiao, S.S.; Yan, X.; Zou, W.; et al. Sedimentary processes dominate nitrous oxide production and emission in the hypoxic zone off the Changjiang River estuary. *Sci. Total Environ.* **2022**, *827*, 154042. [CrossRef]
52. Maeda, K.; Spor, A.; Edel-Hermann, V.; Heraud, C.; Breuil, M.C.; Bizouard, F.; Toyoda, S.; Yoshida, N.; Steinberg, C.; Philippot, L. N_2O production, a widespread trait in fungi. *Sci. Rep.* **2015**, *5*, 9697. [CrossRef]
53. Su, X.; Wen, T.; Wang, Y.; Xu, J.; Cui, L.; Zhang, J.; Xue, X.; Ding, K.; Tang, Y.; Zhu, Y.-g. Stimulation of N_2O emission via bacterial denitrification driven by acidification in estuarine sediments. *Glob. Chang. Biol.* **2021**, *27*, 5564–5579. [CrossRef] [PubMed]
54. Wei, J.; Zhang, X.; Xia, L.; Yuan, W.; Zhou, Z.; Bruggmann, N. Role of chemical reactions in the nitrogenous trace gas emissions and nitrogen retention: A meta-analysis. *Sci. Total Environ.* **2022**, *808*, 152141. [CrossRef] [PubMed]
55. Wei, J.; Amelung, W.; Lehndorff, E.; Schloter, M.; Vereecken, H.; Brüggemann, N. N_2O and NOx emissions by reactions of nitrite with soil organic matter of a Norway spruce forest. *Biogeochemistry* **2017**, *132*, 325–342. [CrossRef]
56. Buchwald, C.; Grabb, K.; Hansel, C.M.; Wankel, S.D. Constraining the role of iron in environmental nitrogen transformations: Dual stable isotope systematics of abiotic NO_2^- reduction by Fe(II) and its production of N_2O. *Geochim. Cosmochim. Acta* **2016**, *186*, 1–12. [CrossRef]

57. Jones, L.C.; Peters, B.; Lezama Pacheco, J.S.; Casciotti, K.L.; Fendorf, S. Stable isotopes and iron oxide mineral products as markers of chemodenitrification. *Environ. Sci. Technol.* **2015**, *49*, 3444–3452. [CrossRef]
58. Picardal, F. Abiotic and Microbial Interactions during Anaerobic Transformations of Fe(II) and NO_x^-. *Front. Microbiol.* **2012**, *3*, 112. [CrossRef]
59. Wankel, S.D.; Ziebis, W.; Buchwald, C.; Charoenpong, C.; de Beer, D.; Dentinger, J.; Xu, Z.; Zengler, K. Evidence for fungal and chemodenitrification based N_2O flux from nitrogen impacted coastal sediments. *Nat. Commun.* **2017**, *8*, 15595. [CrossRef]
60. Wei, J.; Knicker, H.; Zhou, Z.; Eckhardt, K.-U.; Leinweber, P.; Wissel, H.; Yuan, W.; Brüggemann, N. Nitrogen immobilization caused by chemical formation of black- and amide-N in soil. *Geoderma* **2023**, *429*, 116274. [CrossRef]
61. Grabb, K.C.; Buchwald, C.; Hansel, C.M.; Wankel, S.D. A dual nitrite isotopic investigation of chemodenitrification by mineral-associated Fe(II) and its production of nitrous oxide. *Geochim. Cosmochim. Acta* **2017**, *196*, 388–402. [CrossRef]
62. Peters, B.; Casciotti, K.L.; Samarkin, V.A.; Madigan, M.T.; Schutte, C.A.; Joye, S.B. Stable isotope analyses of NO_2^-, NO_3^-, and N_2O in the hypersaline ponds and soils of the McMurdo Dry Valleys, Antarctica. *Geochim. Cosmochim. Acta* **2014**, *135*, 87–101. [CrossRef]
63. Zhu-Barker, X.; Cavazos, A.R.; Ostrom, N.E.; Horwath, W.R.; Glass, J.B. The importance of abiotic reactions for nitrous oxide production. *Biogeochemistry* **2015**, *126*, 251–267. [CrossRef]
64. Cavazos, A.R.; Taillefert, M.; Tang, Y.; Glass, J.B. Kinetics of nitrous oxide production from hydroxylamine oxidation by birnessite in seawater. *Mar. Chem.* **2018**, *202*, 49–57. [CrossRef]
65. Su, X.; Yang, L.; Yang, K.; Tang, Y.; Wen, T.; Wang, Y.; Rillig, M.C.; Rohe, L.; Pan, J.; Li, H.; et al. Estuarine plastisphere as an overlooked source of N_2O production. *Nat. Commun.* **2022**, *13*, 3884. [CrossRef] [PubMed]
66. Gerardo-Nieto, O.; Vega-Penaranda, A.; Gonzalez-Valencia, R.; Alfano-Ojeda, Y.; Thalasso, F. Continuous Measurement of Diffusive and Ebullitive Fluxes of Methane in Aquatic Ecosystems by an Open Dynamic Chamber Method. *Environ. Sci. Technol.* **2019**, *53*, 5159–5167. [CrossRef] [PubMed]
67. Hinshaw, S.E.; Dahlgren, R.A. Dissolved nitrous oxide concentrations and fluxes from the eutrophic San Joaquin River, California. *Environ. Sci. Technol.* **2013**, *47*, 1313–1322. [CrossRef]
68. Zhang, L.; Zhang, S.; Xia, X.; Battin, T.J.; Liu, S.; Wang, Q.; Liu, R.; Yang, Z.; Ni, J.; Stanley, E.H. Unexpectedly minor nitrous oxide emissions from fluvial networks draining permafrost catchments of the East Qinghai-Tibet Plateau. *Nat. Commun.* **2022**, *13*, 950. [CrossRef] [PubMed]
69. Beaulieu, J.J.; Shuster, W.D.; Rebholz, J.A. Nitrous Oxide Emissions from a Large, Impounded River: The Ohio River. *Environ. Sci. Technol.* **2010**, *44*, 7527–7533. [CrossRef]
70. Webb, J.R.; Clough, T.J.; Quayle, W.C. A review of indirect N_2O emission factors from artificial agricultural waters. *Environ. Res. Lett.* **2021**, *16*, 043005. [CrossRef]
71. Yang, W.B.; Yuan, C.S.; Huang, B.Q.; Tong, C.; Yang, L. Emission Characteristics of Greenhouse Gases and Their Correlation with Water Quality at an Estuarine Mangrove Ecosystem—The Application of an In-situ On-site NDIR Monitoring Technique. *Wetlands* **2018**, *38*, 723–738. [CrossRef]
72. Denmead, O.T. Approaches to measuring fluxes of methane and nitrous oxide between landscapes and the atmosphere. *Plant Soil* **2008**, *309*, 5–24. [CrossRef]
73. Wu, S.; Chen, J.; Li, C.; Kong, D.; Yu, K.; Liu, S.; Zou, J. Diel and seasonal nitrous oxide fluxes determined by floating chamber and gas transfer equation methods in agricultural irrigation watersheds in southeast China. *Environ. Monit. Assess.* **2018**, *190*, 122. [CrossRef] [PubMed]
74. Gao, J.; Zheng, X.; Wang, R.; Liao, T.; Zou, J. Preliminary Comparison of the Static Floating Chamber and the Diffusion Model Methods for Measuring Water–Atmosphere Exchanges of Methane and Nitrous Oxide from Inland Water Bodies. *Clim. Environ. Res.* **2014**, *19*, 290–302. (In Chinese) [CrossRef]
75. Clough, T.J.; Bertram, J.E.; Sherlock, R.R.; Leonard, R.L.; Nowicki, B.L. Comparison of measured and $EF_{5\text{-}r}$-derived N_2O fluxes from a spring-fed river. *Glob. Chang. Biol.* **2006**, *12*, 477–488. [CrossRef]
76. Liu, S.; Gao, Q.; Wu, J.; Xie, Y.; Yang, Q.; Wang, R.; Zhang, J.; Liu, Q. Spatial distribution and influencing mechanism of CO_2, N_2O and CH_4 in the Pearl River Estuary in summer. *Sci. Total Environ.* **2022**, *846*, 157381. [CrossRef] [PubMed]
77. Xia, X.; Zhang, L.; Wang, G.; Wang, J.; Zhang, L.; Zhang, S.; Li, Z. Nitrogen loss from a turbid river network based on N_2 and N_2O fluxes: Importance of suspended sediment. *Sci. Total Environ.* **2021**, *757*, 143918. [CrossRef] [PubMed]
78. Rosamond, M.S.; Thuss, S.J.; Schiff, S.L. Dependence of riverine nitrous oxide emissions on dissolved oxygen levels. *Nat. Geosci.* **2012**, *5*, 715–718. [CrossRef]
79. Tian, H.; Xu, R.; Canadell, J.G.; Thompson, R.L.; Winiwarter, W.; Suntharalingam, P.; Davidson, E.A.; Ciais, P.; Jackson, R.B.; Janssens-Maenhout, G.; et al. A comprehensive quantification of global nitrous oxide sources and sinks. *Nature* **2020**, *586*, 248–256. [CrossRef] [PubMed]
80. Yu, Z.; Deng, H.; Wang, D.; Ye, M.; Tan, Y.; Li, Y.; Chen, Z.; Xu, S. Nitrous oxide emissions in the Shanghai river network: Implications for the effects of urban sewage and IPCC methodology. *Glob. Chang. Biol.* **2013**, *19*, 2999–3010. [CrossRef]
81. Jiang, L.Q.; Cai, W.J.; Wang, Y. A comparative study of carbon dioxide degassing in river- and marine-dominated estuaries. *Limnol. Oceanogr.* **2008**, *53*, 2603–2615. [CrossRef]
82. Borges, A.V.; Vanderborght, J.-P.; Schiettecatte, L.-S.; Gazeau, F.; Ferrón-Smith, S.; Delille, B.; Frankignoulle, M. Variability of the gas transfer velocity of CO_2 in a macrotidal estuary (the Scheldt). *Estuaries* **2004**, *27*, 593–603. [CrossRef]

83. Yu, Z.; Wang, D.; Li, Y.; Deng, H.; Hu, B.; Ye, M.; Zhou, X.; Da, L.; Chen, Z.; Xu, S. Carbon dioxide and methane dynamics in a human-dominated lowland coastal river network (Shanghai, China). *J. Geophys. Res. Biogeosciences* **2017**, *122*, 1738–1758. [CrossRef]
84. Aho, K.S.; Fair, J.H.; Hosen, J.D.; Kyzivat, E.D.; Logozzo, L.A.; Weber, L.C.; Yoon, B.; Zarnetske, J.P.; Raymond, P.A. An intense precipitation event causes a temperate forested drainage network to shift from N_2O source to sink. *Limnol. Oceanogr.* **2022**, *67*, S242–S257. [CrossRef]
85. IPCC. *2019 Refinement to the 2006 IPCC Guidelines for National Greenhouse Gas Inventories. Volume 4 Agriculture, Forestry and Other Land Use. Chapter 11: N_2O Emissions from Managed Soils, and CO_2 Emissions from Lime and Urea Application*; IPCC: Geneva, Switzerland, 2019.
86. IPCC. *2006 IPCC Guidelines for National Greenhouse Gas Inventories. Volume 4: Agriculture, Forestry and Other Land Use*; IPCC: Geneva, Switzerland, 2006.
87. Zhou, Y.; Huang, M.; Tian, H.; Xu, R.; Ge, J.; Yang, X.; Liu, R.; Sun, Y.; Pan, S.; Gao, Q.; et al. Four decades of nitrous oxide emission from Chinese aquaculture underscores the urgency and opportunity for climate change mitigation. *Environ. Res. Lett.* **2021**, *16*, 114038. [CrossRef]
88. Wang, J.; Chen, N.; Yan, W.; Wang, B.; Yang, L. Effect of dissolved oxygen and nitrogen on emission of N_2O from rivers in China. *Atmos. Environ.* **2015**, *103*, 347–356. [CrossRef]
89. Wang, J.; Wang, G.; Zhang, S.; Xin, Y.; Jiang, C.; Liu, S.; He, X.; McDowell, W.H.; Xia, X. Indirect nitrous oxide emission factors of fluvial networks can be predicted by dissolved organic carbon and nitrate from local to global scales. *Glob. Chang. Biol.* **2022**, *28*, 7270–7285. [CrossRef] [PubMed]
90. Hu, M.; Chen, D.; Dahlgren, R.A. Modeling nitrous oxide emission from rivers: A global assessment. *Glob. Chang. Biol.* **2016**, *22*, 3566–3582. [CrossRef] [PubMed]
91. Outram, F.N.; Hiscock, K.M. Indirect nitrous oxide emissions from surface water bodies in a lowland arable catchment: A significant contribution to agricultural greenhouse gas budgets? *Environ. Sci. Technol.* **2012**, *46*, 8156–8163. [CrossRef] [PubMed]
92. Liu, F.; Zhu, Q.; Wang, Y.; Lai, X.; Liao, K.; Guo, C. Storages and leaching losses of soil water dissolved CO_2 and N_2O on typical land use hillslopes in southeastern hilly area of China. *Sci. Total Environ.* **2023**, *886*, 163780. [CrossRef]
93. Hama-Aziz, Z.Q.; Hiscock, K.M.; Cooper, R.J. Indirect Nitrous Oxide Emission Factors for Agricultural Field Drains and Headwater Streams. *Environ. Sci. Technol.* **2017**, *51*, 301–307. [CrossRef]
94. Zhou, Y.; Toyoda, R.; Suenaga, T.; Aoyagi, T.; Hori, T.; Terada, A. Low nitrous oxide concentration and spatial microbial community transition across an urban river affected by treated sewage. *Water Res.* **2022**, *216*, 118276. [CrossRef]
95. Garnier, J.; Billen, G.; Vilain, G.; Martinez, A.; Silvestre, M.; Mounier, E.; Toche, F. Nitrous oxide (N_2O) in the Seine river and basin: Observations and budgets. *Agric. Ecosyst. Environ.* **2009**, *133*, 223–233. [CrossRef]
96. Hu, M.; Li, B.; Wu, K.; Zhang, Y.; Wu, H.; Zhou, J.; Chen, D. Modeling Riverine N_2O Sources, Fates, and Emission Factors in a Typical River Network of Eastern China. *Environ. Sci. Technol.* **2021**, *55*, 13356–13365. [CrossRef] [PubMed]
97. Tian, L.; Cai, Y.; Akiyama, H. A review of indirect N_2O emission factors from agricultural nitrogen leaching and runoff to update of the default IPCC values. *Environ. Pollut.* **2019**, *245*, 300–306. [CrossRef] [PubMed]
98. Wang, M.; Li, Y.; Lei, K.; Yang, L. Concentration, Flux, and Emission Factor of N_2O in River with Different Nitrogen Pollution Features. *Environ. Sci.* **2018**, *39*, 5400–5409. (In Chinese) [CrossRef]
99. He, Y.; Wang, X.; Chen, H.; Yuan, X.; Wu, N.; Zhang, Y.; Yue, J.; Zhang, Q.; Diao, Y.; Zhou, L. Effect of watershed urbanization on N_2O emissions from the Chongqing metropolitan river network, China. *Atmos. Environ.* **2017**, *171*, 70–81. [CrossRef]
100. Audet, J.; Wallin, M.B.; Kyllmar, K.; Andersson, S.; Bishop, K. Nitrous oxide emissions from streams in a Swedish agricultural catchment. *Agric. Ecosyst. Environ.* **2017**, *236*, 295–303. [CrossRef]
101. Baulch, H.M.; Schiff, S.L.; Thuss, S.J.; Dillon, P.J. Isotopic character of nitrous oxide emitted from streams. *Environ. Sci. Technol.* **2011**, *45*, 4682–4688. [CrossRef] [PubMed]
102. Cooper, R.J.; Wexler, S.K.; Adams, C.A.; Hiscock, K.M. Hydrogeological controls on regional-scale indirect nitrous oxide emission factors for rivers. *Environ. Sci. Technol.* **2017**, *51*, 10440–10448. [CrossRef]
103. Li, X.; Sardans, J.; Qi, M.; Ni, X.; Zhang, M.; Peñuelas, J.; Yue, K.; Wu, F. Nitrous oxide concentration and flux in Min River Basin of southeast China: Effects of land use, stream order and water variables. *J. Hydrol.* **2022**, *614*, 128507. [CrossRef]
104. Qi, M.; Luo, L.; Hong, X.; Qian, W.; Tong, C.; Li, X. Spatial and temporal variations and influencing factors of nitrous oxide emissions from surface water in Min River Estuary. *Acta Sci. Circumstantiae* **2022**, *42*, 489–500. (In Chinese) [CrossRef]
105. Guan, D.; Zhao, H.; Yao, Z. The distribution and flux of nitrous oxide in the Liaohe Estuary area. *Acta Oceanol. Sin.* **2009**, *31*, 85–90. (In Chinese)
106. Li, X.; Yue, F.; Zhou, B.; Wang, X.; Hu, J.; Chen, S.; Li, S. Study on N_2O release from typical gate-controlled rivers in Bohai Bay. *China Environ. Sci.* **2022**, *42*, 356–366. (In Chinese) [CrossRef]
107. Hu, B.; Wang, D.; Zhou, J.; Meng, W.; Li, C.; Sun, Z.; Guo, X.; Wang, Z. Greenhouse gases emission from the sewage draining rivers. *Sci. Total Environ.* **2018**, *612*, 1454–1462. [CrossRef] [PubMed]
108. Xia, Y.; Li, Y.; Li, X.; Guo, M.; She, D.; Yan, X. Diurnal pattern in nitrous oxide emissions from a sewage-enriched river. *Chemosphere* **2013**, *92*, 421–428. [CrossRef]
109. Wu, W.; Wang, J.; Zhou, X.; Yuan, B.; Guo, M.; Ren, L. Spatiotemporal distribution of nitrous oxide (N_2O) emissions from cascade reservoirs in Lancang-Mekong River Yunnan section, Southwestern China. *River Res. Appl.* **2020**, *37*, 1055–1069. [CrossRef]

110. Li, X.; Yu, Y.; Fan, H.; Tang, C. Intense denitrification and sewage effluent result in enriched ^{15}N in N_2O from urban polluted rivers. *J. Hydrol.* **2022**, *608*, 127631. [CrossRef]
111. Lin, H.; Dai, M.; Kao, S.-J.; Wang, L.; Roberts, E.; Yang, J.-Y.T.; Huang, T.; He, B. Spatiotemporal variability of nitrous oxide in a large eutrophic estuarine system: The Pearl River Estuary, China. *Mar. Chem.* **2016**, *182*, 14–24. [CrossRef]
112. Grossel, A.; Bourennane, H.; Ayzac, A.; Pasquier, C.; Henault, C. Indirect emissions of nitrous oxide in a cropland watershed with contrasting hydrology in central France. *Sci. Total Environ.* **2021**, *766*, 142664. [CrossRef]
113. Borges, A.V.; Darchambeau, F.; Lambert, T.; Morana, C.; Allen, G.H.; Tambwe, E.; Sembaito, A.T.; Mambo, T.; Wabakhangazi, J.N.; Descy, J.-P.; et al. Variations in dissolved greenhouse gases (CO_2, CH_4, N_2O) in the Congo River network overwhelmingly driven by fluvial-wetland connectivity. *Biogeosciences* **2019**, *16*, 3801–3834. [CrossRef]
114. Mwanake, R.M.; Gettel, G.M.; Aho, K.S.; Namwaya, D.W.; Masese, F.O.; Butterbach-Bahl, K.; Raymond, P.A. Land Use, Not Stream Order, Controls N_2O Concentration and Flux in the Upper Mara River Basin, Kenya. *J. Geophys. Res. Biogeosci.* **2019**, *124*, 3491–3506. [CrossRef]
115. Hershey, R.; Nandan, S.B.; Jayachandran, P.R.; Vijay, A.; Sudheesh, V. Nitrous oxide flux from a Tropical estuarine system (Cochin estuary, India). *Reg. Stud. Mar. Sci.* **2019**, *30*, 100725. [CrossRef]
116. Nirmal Rajkumar, A.; Barnes, J.; Ramesh, R.; Purvaja, R.; Upstill-Goddard, R.C. Methane and nitrous oxide fluxes in the polluted Adyar River and estuary, SE India. *Mar. Pollut. Bull.* **2008**, *56*, 2043–2051. [CrossRef] [PubMed]
117. Clough, T.J.; Buckthought, L.E.; Casciotti, K.L.; Kelliher, F.M.; Jones, P.K. Nitrous oxide dynamics in a braided river system, New Zealand. *J. Environ. Qual.* **2011**, *40*, 1532–1541. [CrossRef]
118. Gao, X.; Ouyang, W.; Lin, C.; Wang, K.; Hao, F.; Hao, X.; Lian, Z. Considering atmospheric N_2O dynamic in SWAT model avoids the overestimation of N_2O emissions in river networks. *Water Res.* **2020**, *174*, 115624. [CrossRef] [PubMed]
119. Kroeze, C.; Dumont, E.; Seitzinger, S. Future trends in emissions of N_2O from rivers and estuaries. *J. Integr. Environ. Sci.* **2010**, *7*, 71–78. [CrossRef]
120. Maavara, T.; Lauerwald, R.; Laruelle, G.G.; Akbarzadeh, Z.; Bouskill, N.J.; Van Cappellen, P.; Regnier, P. Nitrous oxide emissions from inland waters: Are IPCC estimates too high? *Glob. Chang. Biol.* **2018**, *25*, 473–488. [CrossRef]
121. Tian, H.; Yang, J.; Lu, C.; Xu, R.; Canadell, J.G.; Jackson, R.B.; Arneth, A.; Chang, J.; Chen, G.; Ciais, P.; et al. The Global N_2O Model Intercomparison Project. *Bull. Am. Meteorol. Soc.* **2018**, *99*, 1231–1251. [CrossRef]
122. Wang, C.; Schürz, C.; Zoboli, O.; Zessner, M.; Schulz, K.; Watzinger, A.; Bodner, G.; Mehdi-Schulz, B. N_2O Emissions from Two Austrian Agricultural Catchments Simulated with an N_2O Submodule Developed for the SWAT Model. *Atmosphere* **2021**, *13*, 50. [CrossRef]
123. Marzadri, A.; Dee, M.M.; Tonina, D.; Bellin, A.; Tank, J.L. Role of surface and subsurface processes in scaling N_2O emissions along riverine networks. *Proc. Natl. Acad. Sci. USA* **2017**, *114*, 4330–4335. [CrossRef]
124. Kroeze, C.; Seitzinger, S.P. Nitrogen inputs to rivers, estuaries and continental shelves and related nitrous oxide emissions in 1990 and 2050: A global model. *Nutr. Cycl. Agroecosystems* **1998**, *52*, 195–212. [CrossRef]
125. Reay, D.S.; Davidson, E.A.; Smith, K.A.; Smith, P.; Melillo, J.M.; Dentener, F.; Crutzen, P.J. Global agriculture and nitrous oxide emissions. *Nat. Clim. Chang.* **2012**, *2*, 410–416. [CrossRef]
126. Kroeze, C.; Dumont, E.; Seitzinger, S.P. New estimates of global emissions of N_2O from rivers and estuaries. *Environ. Sci.* **2005**, *2*, 159–165. [CrossRef]
127. Qin, X.; Li, Y.; Goldberg, S.; Wan, Y.; Fan, M.; Liao, Y.; Wang, B.; Gao, Q.; Li, Y. Assessment of Indirect N_2O Emission Factors from Agricultural River Networks Based on Long-Term Study at High Temporal Resolution. *Environ. Sci. Technol.* **2019**, *53*, 10781–10791. [CrossRef] [PubMed]
128. Borges, A.V.; Darchambeau, F.; Teodoru, C.R.; Marwick, T.R.; Tamooh, F.; Geeraert, N.; Omengo, F.O.; Guérin, F.; Lambert, T.; Morana, C.; et al. Globally significant greenhouse-gas emissions from African inland waters. *Nat. Geosci.* **2015**, *8*, 637–642. [CrossRef]
129. Gao, D.; Hou, L.; Li, X.; Liu, M.; Zheng, Y.; Yin, G.; Yang, Y.; Liu, C.; Han, P. Exotic Spartina alterniflora invasion alters soil nitrous oxide emission dynamics in a coastal wetland of China. *Plant Soil* **2019**, *442*, 233–246. [CrossRef]
130. Sutka, R.L.; Ostrom, N.E.; Ostrom, P.H.; Gandhi, H.; Breznak, J.A. Nitrogen isotopomer site preference of N_2O produced by Nitrosomonas europaea and Methylococcus capsulatus Bath. *Rapid Commun. Mass Spectrom.* **2003**, *17*, 738–745. [CrossRef] [PubMed]
131. Denk, T.R.A.; Mohn, J.; Decock, C.; Lewicka-Szczebak, D.; Harris, E.; Butterbach-Bahl, K.; Kiese, R.; Wolf, B. The nitrogen cycle: A review of isotope effects and isotope modeling approaches. *Soil Biol. Biochem.* **2017**, *105*, 121–137. [CrossRef]
132. Sutka, R.L.; Ostrom, N.E.; Ostrom, P.H.; Breznak, J.A.; Gandhi, H.; Pitt, A.J.; Li, F. Distinguishing nitrous oxide production from nitrification and denitrification on the basis of isotopomer abundances. *Appl. Environ. Microbiol.* **2006**, *72*, 638–644. [CrossRef]
133. Sutka, R.L.; Adams, G.C.; Ostrom, N.E.; Ostrom, P.H. Isotopologue fractionation during N_2O production by fungal denitrification. *Rapid Commun. Mass Spectrom.* **2008**, *22*, 3989–3996. [CrossRef]
134. Toyoda, S.; Mutobe, H.; Yamagishi, H.; Yoshida, N.; Tanji, Y. Fractionation of N_2O isotopomers during production by denitrifier. *Soil Biol. Biochem.* **2005**, *37*, 1535–1545. [CrossRef]
135. Schmidt, I.; van Spanning, R.J.; Jetten, M.S. Denitrification and ammonia oxidation by Nitrosomonas europaea wild-type, and NirK- and NorB-deficient mutants. *Microbiology* **2004**, *150*, 4107–4114. [CrossRef] [PubMed]

136. Ma, P.; Li, X.; Chen, F.; Liu, S.; Hou, C. The isotopomer ratios of N_2O in the Shaying River, the upper Huai River network, Eastern China: The significances of mechanisms and productions of N_2O in the heavy ammonia polluted rivers. *Sci. Total Environ.* **2019**, *687*, 1315–1326. [CrossRef]
137. Heil, J.; Wolf, B.; Brüggemann, N.; Emmenegger, L.; Tuzson, B.; Vereecken, H.; Mohn, J. Site-specific ^{15}N isotopic signatures of abiotically produced N_2O. *Geochim. Cosmochim. Acta* **2014**, *139*, 72–82. [CrossRef]
138. Li, Y.H.; Peng, T.H.; Broecker, W.S.; Ostlund, H.C. The average vertical mixing coefficient for the oceanic thermocline. *Tellus B Chem. Phys. Meteorol.* **1984**, *36*, 212. [CrossRef]
139. Toyoda, S.; Kuroki, N.; Yoshida, N.; Ishijima, K.; Tohjima, Y.; Machida, T. Decadal time series of tropospheric abundance of N_2O isotopomers and isotopologues in the Northern Hemisphere obtained by the long-term observation at Hateruma Island, Japan. *J. Geophys. Res. Atmos.* **2013**, *118*, 3369–3381. [CrossRef]
140. Yoshida, N.; Toyoda, S. Constraining the atmospheric N_2O budget from intramolecular site preference in N_2O isotopomers. *Nature* **2000**, *405*, 330–334. [CrossRef]